Electronic Supplementary Information

Correlation between Electroconductive and Structural Properties of Proton Conductive Acceptor-Doped Barium Zirconate

Donglin Han [a*], Kozo Shinoda [b], Shigeo Sato [c], Masatoshi Majima [d], Tetsuya Uda [a*]

[a] Department of Materials Science and Engineering, Kyoto University,
Yoshida Honmachi, Sakyo-ku, Kyoto 606-8501, Japan

[b] Institute of Multidisciplinary Research for Advanced Materials, Tohoku University,
Katahira 2-1-1, Aoba-ku, Sendai 980-8577, Japan

[c] Graduate School of Science and Engineering, Ibaraki University
4-12-1 Nakanarusawa, Hitachi 316-8511, Japan

[d] Sumitomo Electric Industries, Ltd.,
1-1-1, Koyakita, Itami-shi, Hyogo 664-0016, Japan

* Corresponding author: Donglin Han (han.donglin.8n@kyoto-u.ac.jp)
and Tetsuya Uda (materials_process@aqua.mtl.kyoto-u.ac.jp)
TEL: +81-75-753-5445, FAX: +81-75-753-5284
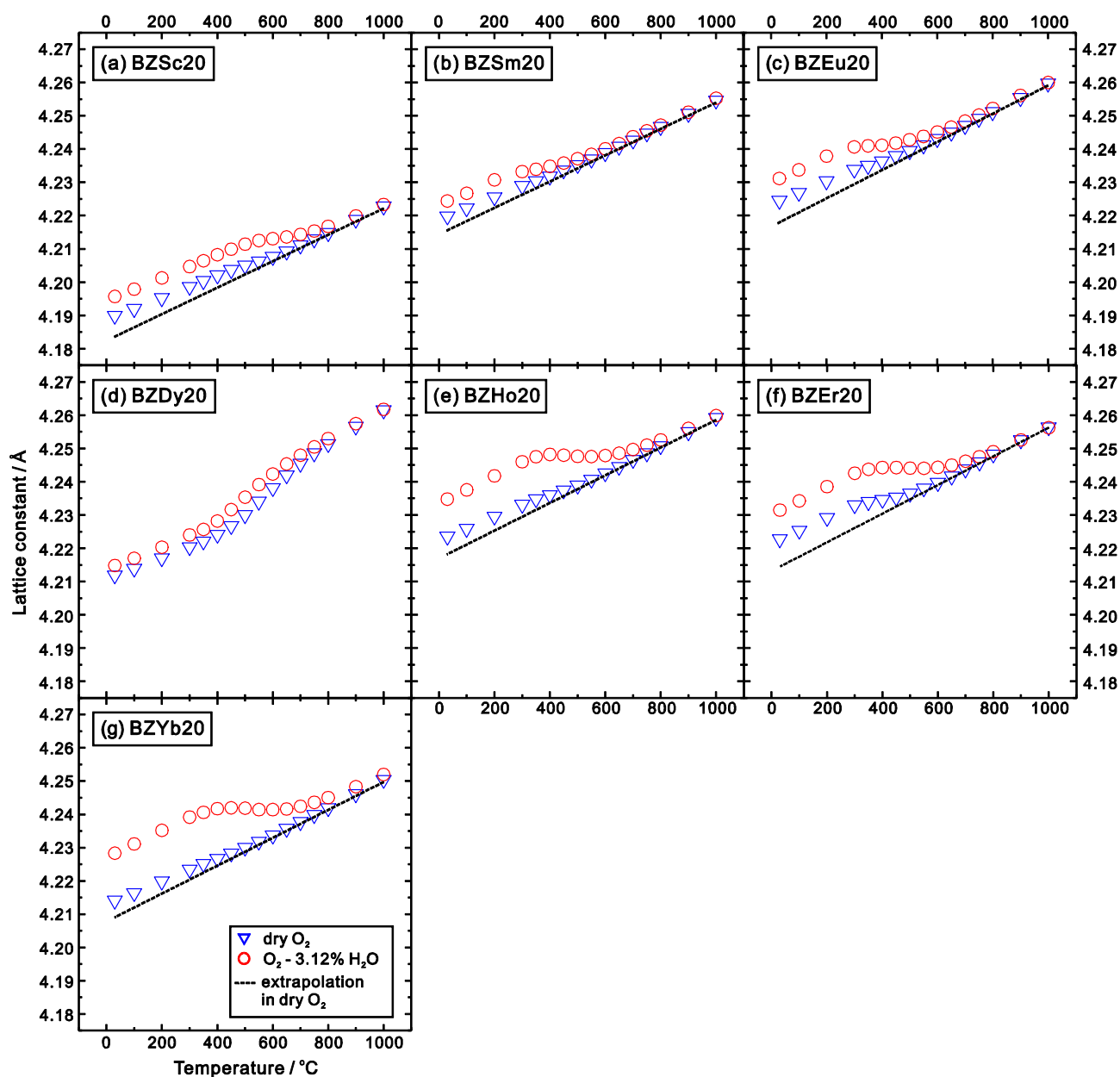
Fig. S1 Variation of lattice constants of (a) $BaZr_{0.8}Sc_{0.2}O_{3-\delta}$ (BZSc20), (b) $BaZr_{0.8}Sm_{0.2}O_{3-\delta}$ (BZSm20), (c) $BaZr_{0.8}Eu_{0.2}O_{3-\delta}$ (BZEu20), (d) $BaZr_{0.8}Dy_{0.2}O_{3-\delta}$ (BZDy20), (e) $BaZr_{0.8}Ho_{0.2}O_{3-\delta}$ (BZHo20), (f) $BaZr_{0.8}Er_{0.2}O_{3-\delta}$ (BZEr20), and (g) $BaZr_{0.8}Yb_{0.2}O_{3-\delta}$ (BZYb20) in dry O_2 and wet O_2 ($p_{H_2O} = 0.0312\ atm$) with temperature. All the samples were finally heat-treatment at 1600 °C in O_2 for 24 h for sintering. The dashed line indicates the extrapolation using the data obtained in the temperature range of 700 to 1000 °C in dry O_2. The profile of BZSc20, BZSm20, BZEu20 and BZDy20 were cited from our previous work (D. Han, *et al.*, *J. Am. Ceram. Soc.*, 2014, **97**, 643.).
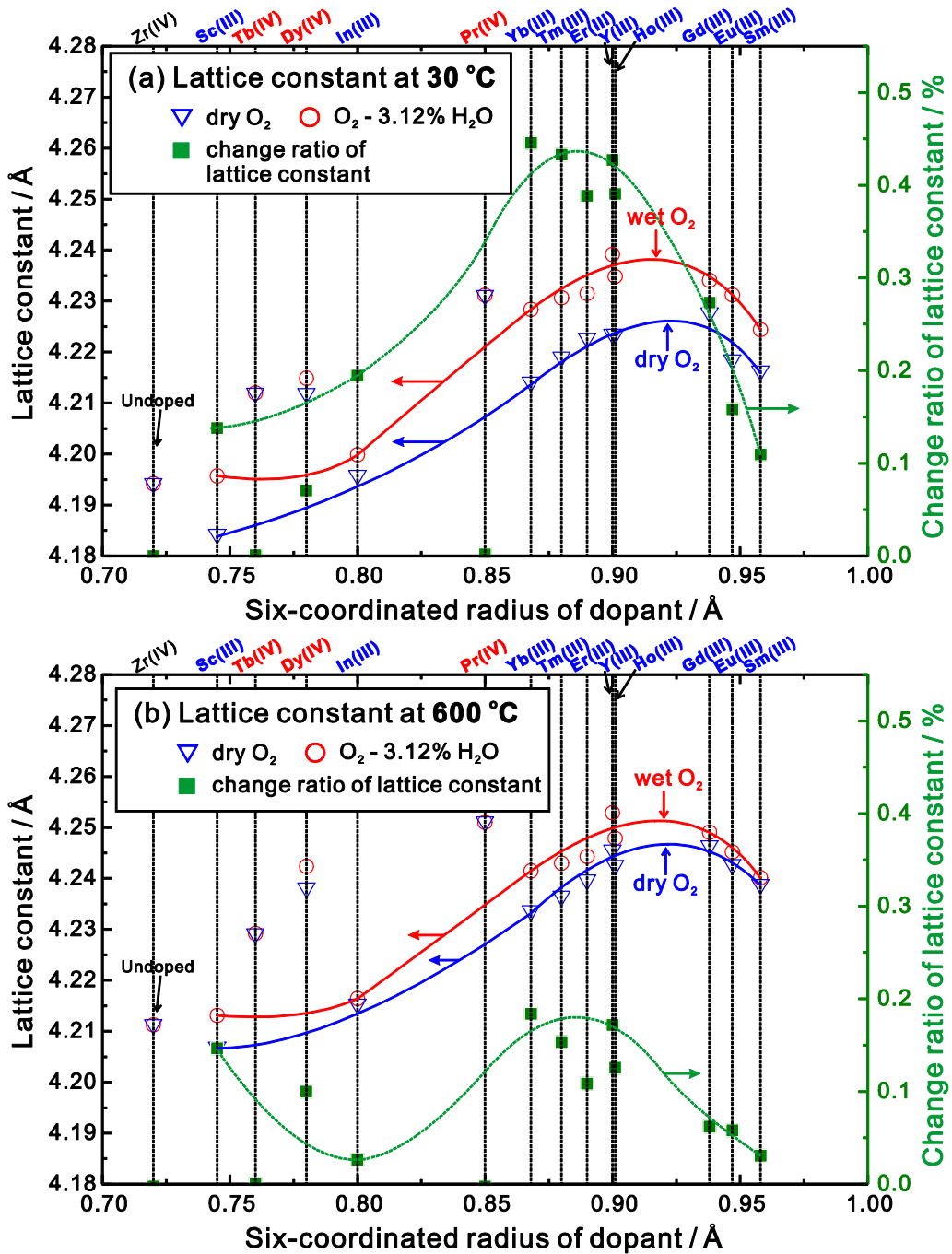
Fig. S2 Lattice constant of the samples of undoped $BaZrO_3$ and those doped with rare earth elements and In at (a) 30 °C, and (b) 600 °C, determined from HT-XRD measurements. The lattice constants in dry and wet O_2 ($p_{H_2O} = 0.0312$ atm) atmospheres were marked using open triangle and circle, respectively. Change ratio of the lattice constant was marked using solid square symbols. All the samples were sintered at 1600 °C in O_2 for 24 h before the HT-XRD measurements. Solid and dash lines are used to highlight the tendency of variation with the increasing dopant radius for the lattice constants of the samples doped with trivalent cations (Sc, In, Yb, Tm, Er, Y, Ho, Gd, Eu and Sm) and their change ratio.
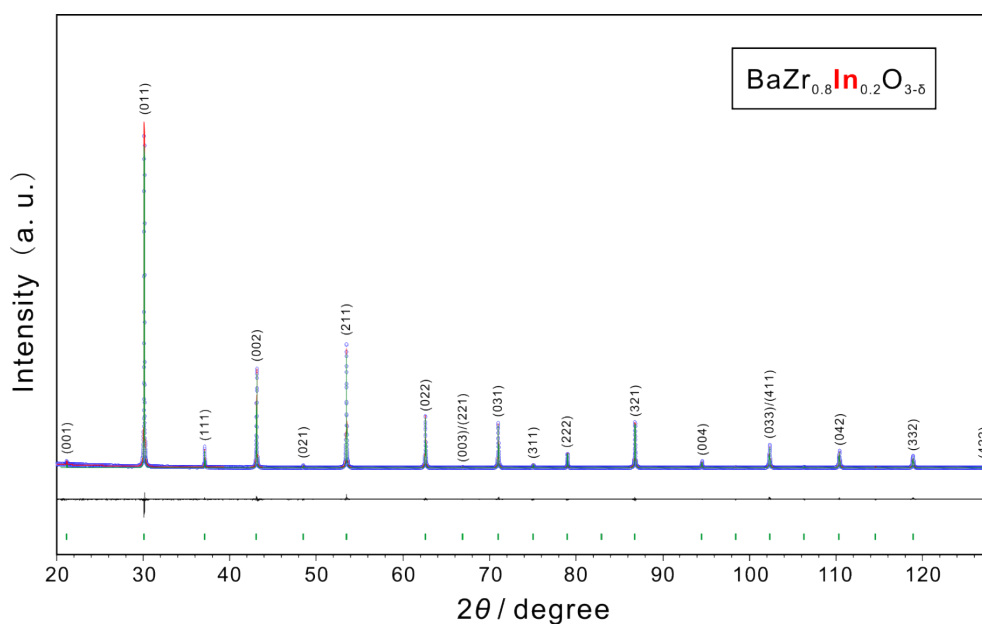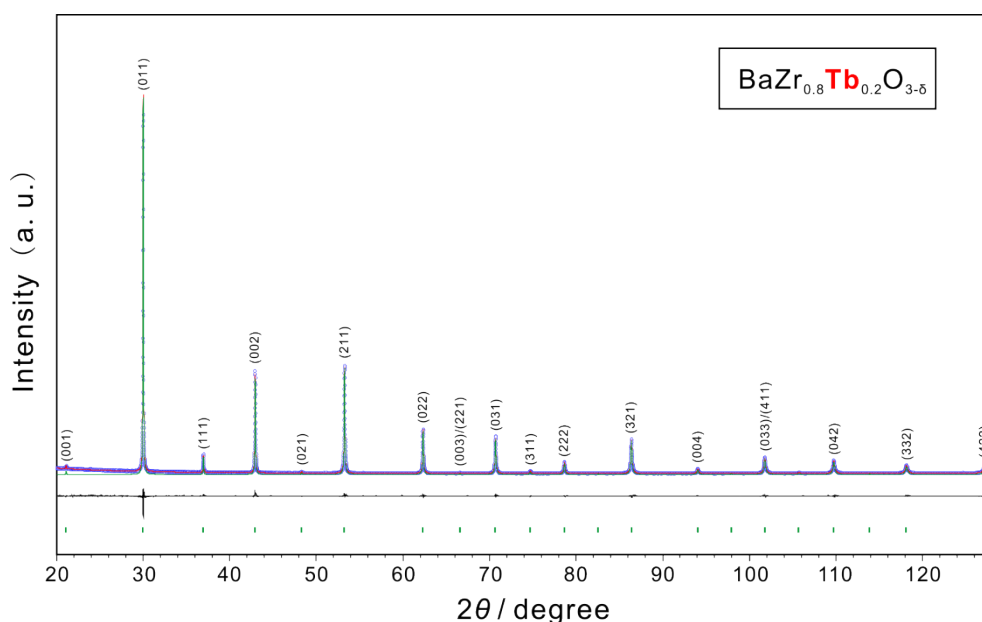
Fig. S3 Rietveld refinement of the diffraction pattern of $BaZr_{0.8}In_{0.2}O_{3-\delta}$ collected with Cu $K\alpha_1$ monochromatic X-ray. The sample was quenched to room temperature after the heat-treatment at 1600 °C. Two cubic perovskite ($Pm\overline{3}m$) structure models for hydrated and dehydrated phases were adopted for the refinement. Observed profile (blue circle), calculated profile (red line), difference (black line at bottom), and Bragg peaks of candidate phases (vertical lines) are shown.
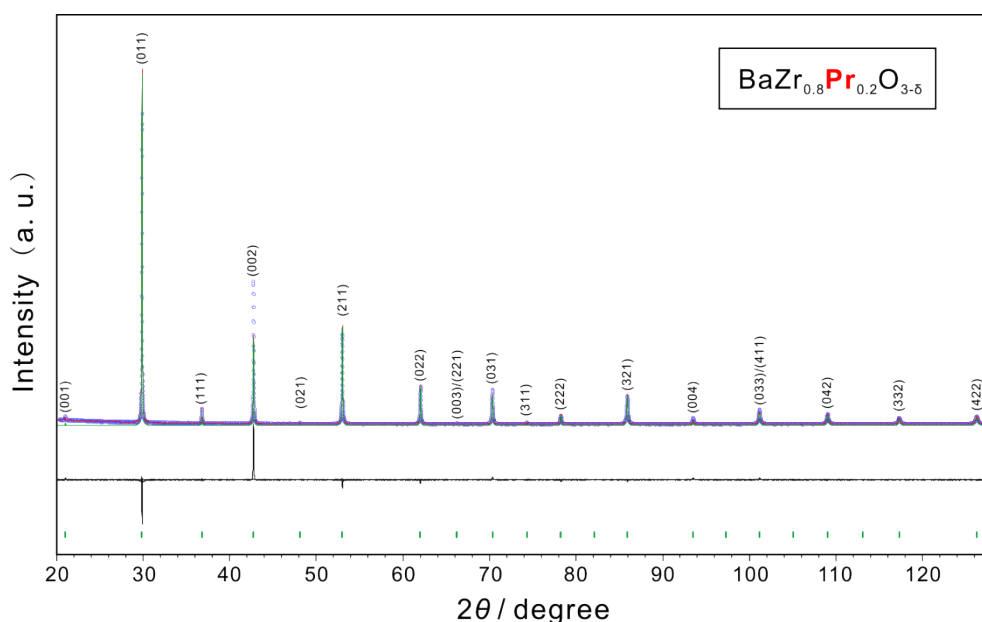
Fig. S4 Rietveld refinement of the diffraction pattern of $BaZr_{0.8}Pr_{0.2}O_{3-\delta}$ collected with Cu $K\alpha_1$ monochromatic X-ray. The sample was quenched to room temperature after the heat-treatment at 1600 °C. One cubic perovskite ($Pm\overline{3}m$) structure model was adopted for the refinement. Observed profile (blue circle), calculated profile (red line), difference (black line at bottom), and Bragg peaks of candidate phases (vertical lines) are shown.
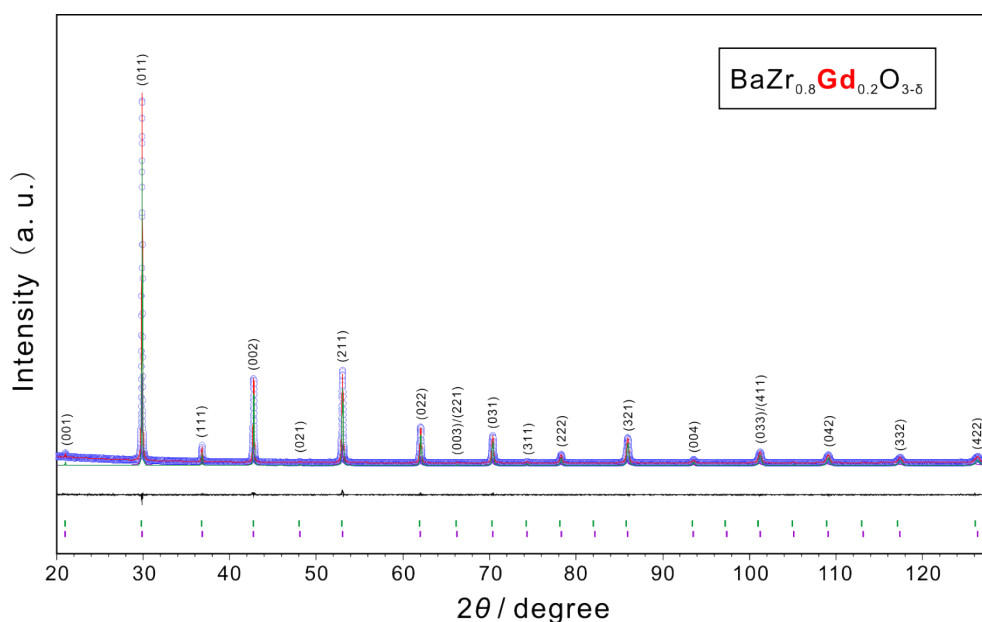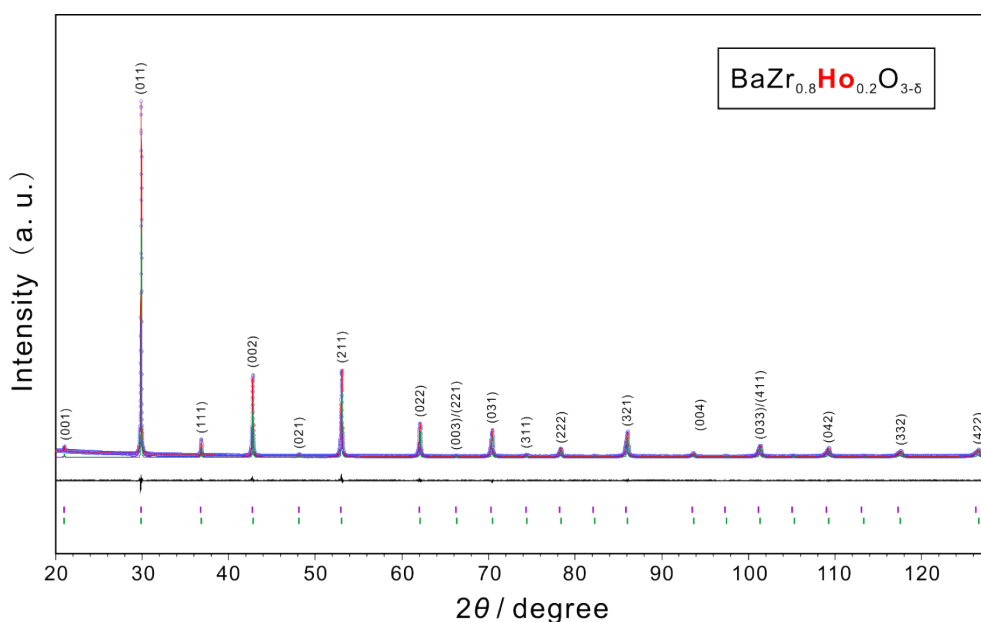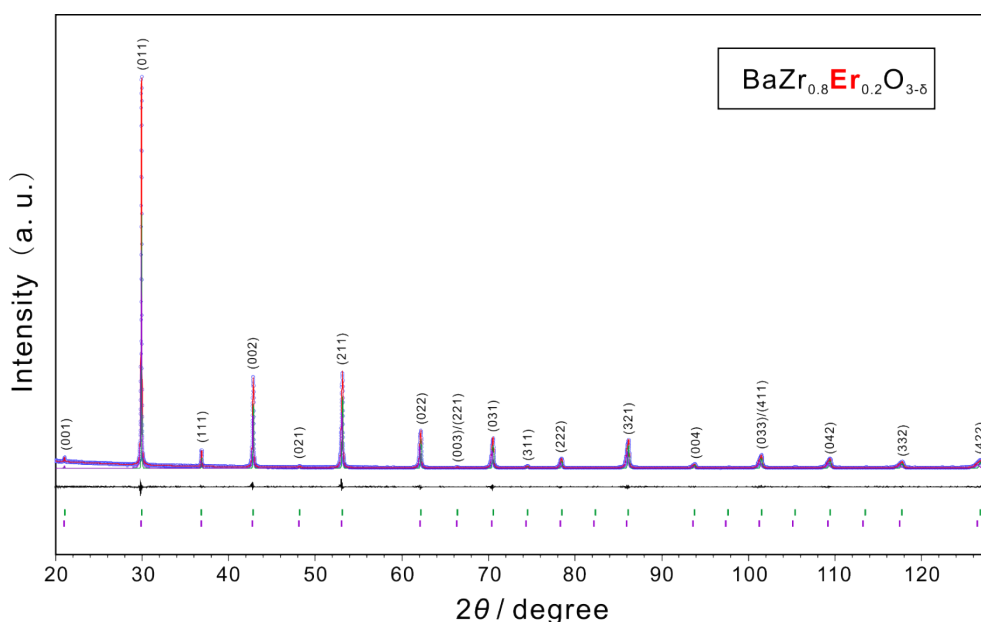
Fig. S5 Rietveld refinement of the diffraction pattern of $BaZr_{0.8}Gd_{0.2}O_{3-\delta}$ collected with Cu $K\alpha_1$ monochromatic X-ray. The sample was quenched to room temperature after the heat-treatment at 1600 ^oC. Two cubic perovskite ($Pm\overline{3}m$) structure models for hydrated and dehydrated phases were adopted for the refinement. Observed profile (blue circle), calculated profile (red line), difference (black line at bottom), and Bragg peaks of candidate phases (vertical lines) are shown.

Fig. S6 Rietveld refinement of the diffraction pattern of $BaZr_{0.8}Tb_{0.2}O_{3-\delta}$ collected with Cu $K\alpha_1$ monochromatic X-ray. The sample was quenched to room temperature after the heat-treatment at 1600 ^oC. One cubic perovskite ($Pm\overline{3}m$) structure model was adopted for the refinement. Observed profile (blue circle), calculated profile (red line), difference (black line at bottom), and Bragg peaks of candidate phases (vertical lines) are shown.
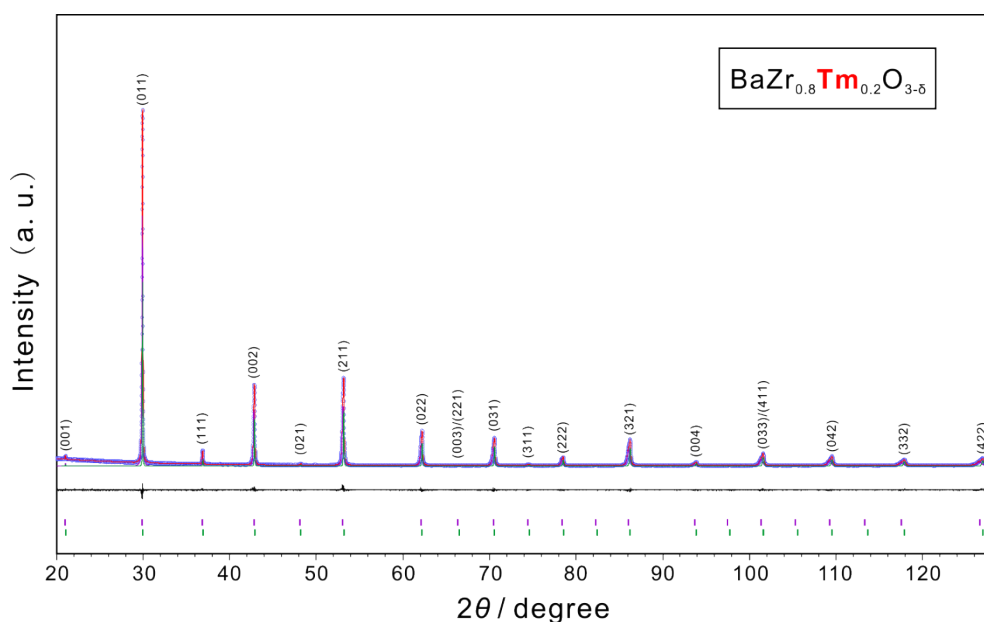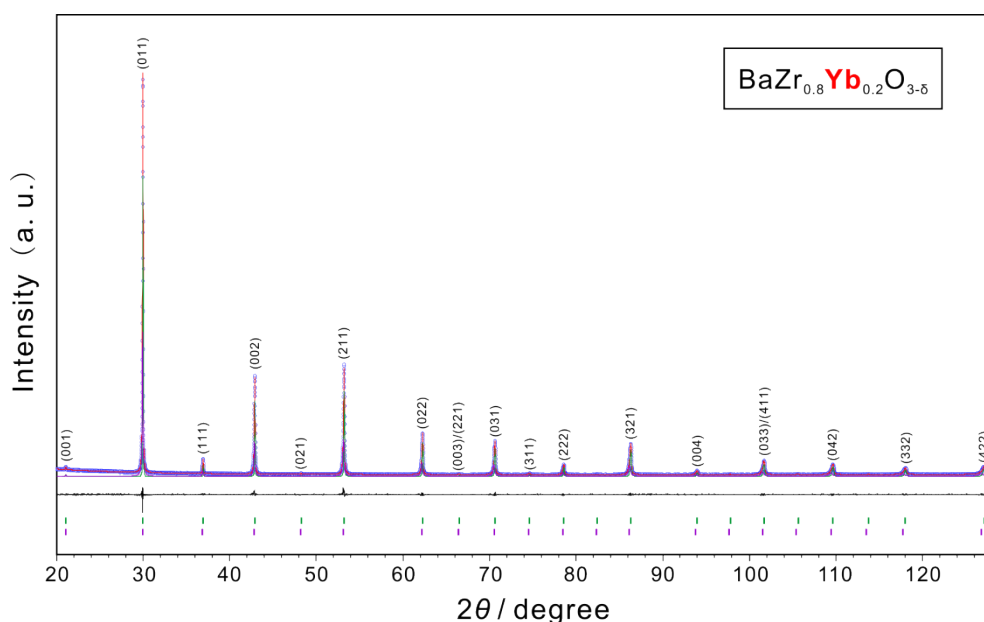
Fig. S7 Rietveld refinement of the diffraction pattern of $BaZr_{0.8}Ho_{0.2}O_{3-\delta}$ collected with Cu $K\alpha_1$ monochromatic X-ray. The sample was quenched to room temperature after the heat-treatment at 1600 ºC. Two cubic perovskite ($Pm\overline{3}m$) structure models for hydrated and dehydrated phases were adopted for the refinement. Observed profile (blue circle), calculated profile (red line), difference (black line at bottom), and Bragg peaks of candidate phases (vertical lines) are shown.


Fig. S8 Rietveld refinement of the diffraction pattern of $BaZr_{0.8}Er_{0.2}O_{3-\delta}$ collected with Cu $K\alpha_1$ monochromatic X-ray. The sample was quenched to room temperature after the heat-treatment at 1600 ºC. Two cubic perovskite ($Pm\overline{3}m$) structure models for hydrated and dehydrated phases were adopted for the refinement. Observed profile (blue circle), calculated profile (red line), difference (black line at bottom), and Bragg peaks of candidate phases (vertical lines) are shown.

Fig. S9 Rietveld refinement of the diffraction pattern of $BaZr_{0.8}Tm_{0.2}O_{3-\delta}$ collected with Cu $K\alpha_1$ monochromatic X-ray. The sample was quenched to room temperature after the heat-treatment at 1600 °C. Two cubic perovskite ($Pm\overline{3}m$) structure models for hydrated and dehydrated phases were adopted for the refinement. Observed profile (blue circle), calculated profile (red line), difference (black line at bottom), and Bragg peaks of candidate phases (vertical lines) are shown.


Fig. S10 Rietveld refinement of the diffraction pattern of $BaZr_{0.8}Yb_{0.2}O_{3-\delta}$ collected with Cu $K\alpha_1$ monochromatic X-ray. The sample was quenched to room temperature after the heat-treatment at 1600 °C. Two cubic perovskite ($Pm\overline{3}m$) structure models for hydrated and dehydrated phases were adopted for the refinement. Observed profile (blue circle), calculated profile (red line), difference (black line at bottom), and Bragg peaks of candidate phases (vertical lines) are shown.

7
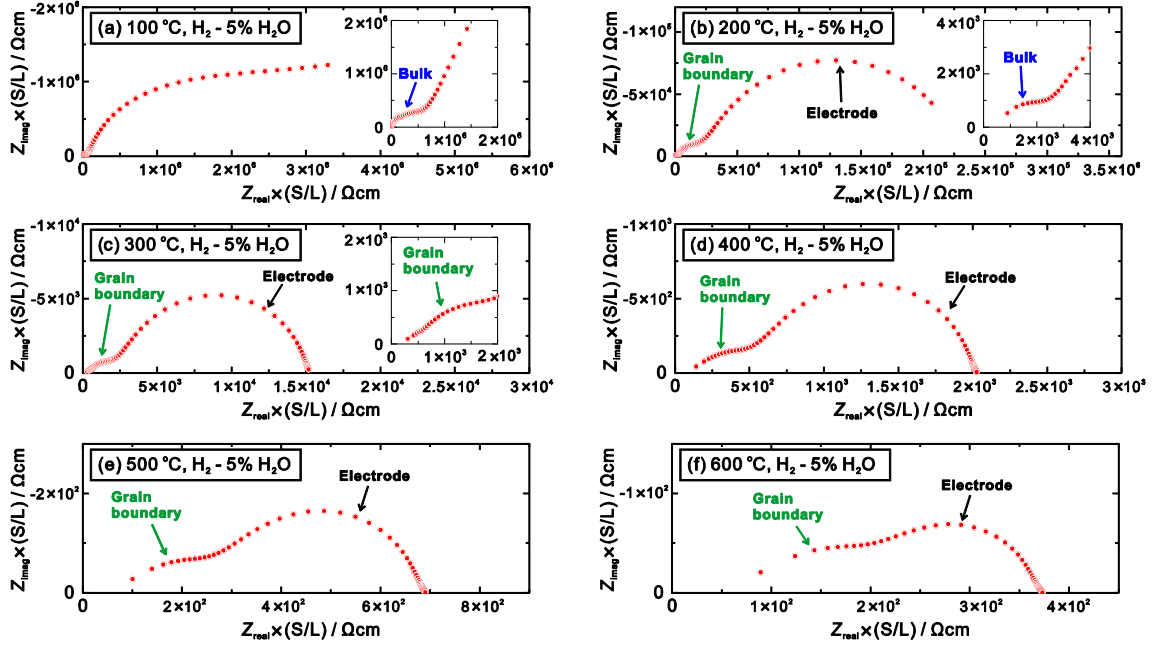
Fig. S11 AC impedance spectra of BaZr$_{0.8}$Y$_{0.2}$O$_{3-\delta}$ in wet H$_2$ ($p_{H_2O} = 0.05$ atm) at various temperature. Semicircle due to the contribution from bulk conduction can be separated at 100 and 200 $^{\circ}$C, but cannot be separated at higher temperature, at which only the contributions from grain boundary conduction and electrode reaction can be identified.
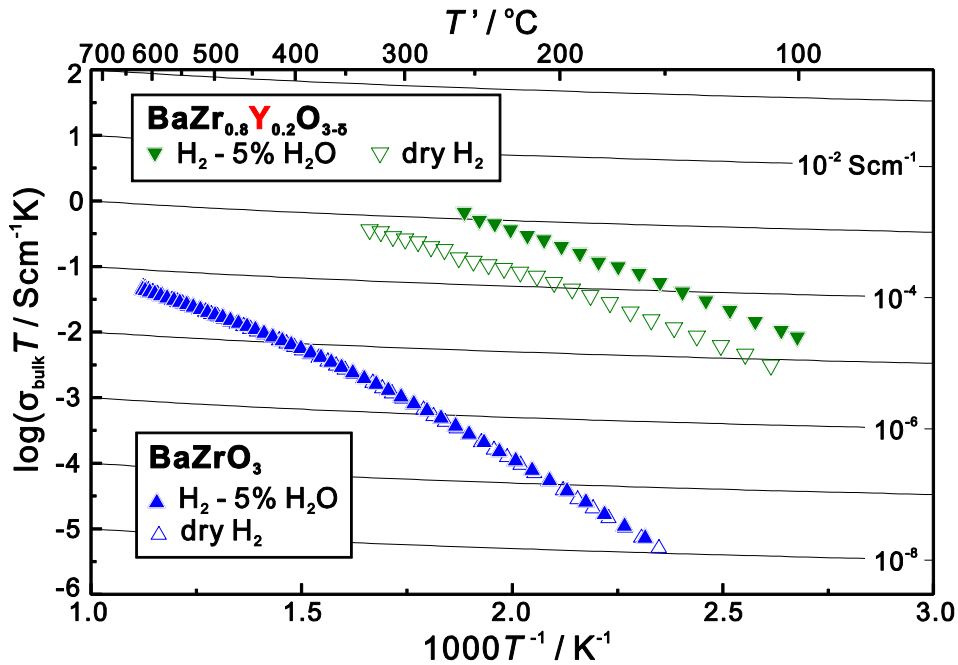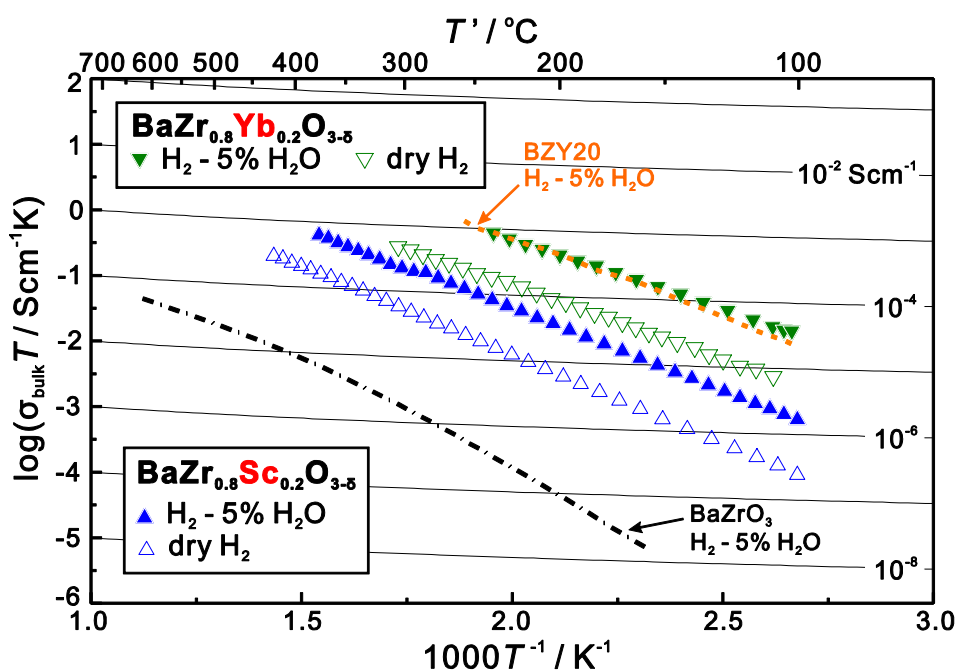

Fig. S12 Arrhenius plots of bulk conductivity of BaZr$_{0.8}$Y$_{0.2}$O$_{3-\delta}$ and undoped BaZrO$_3$ in dry and wet ($p_{H_2O} = 0.05$ atm) atmospheres of H$_2$.
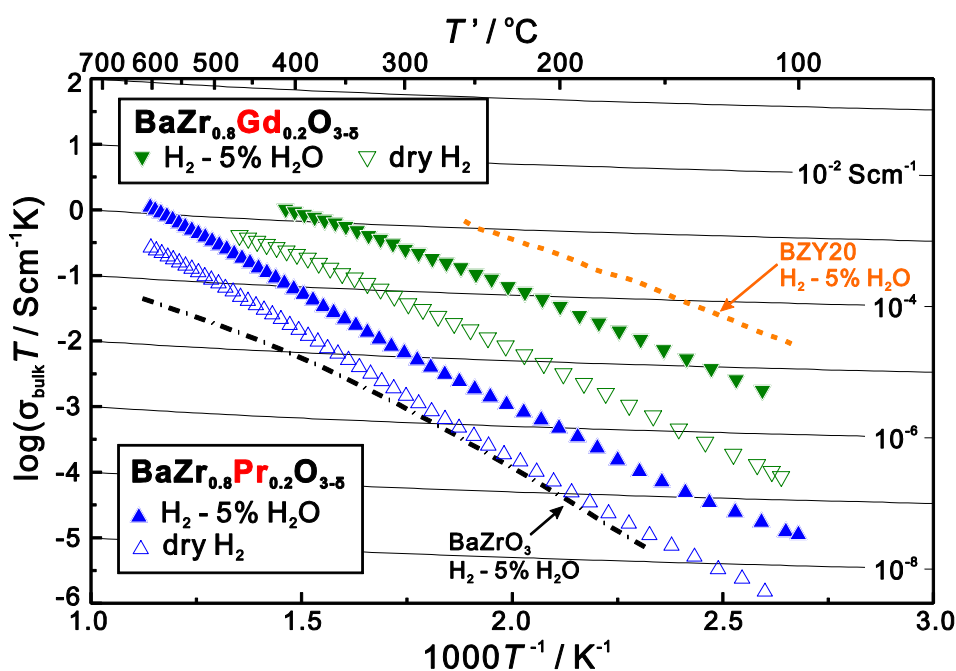
Fig. S13 Arrhenius plots of bulk conductivity of $BaZr_{0.8}Gd_{0.2}O_{3-\delta}$ and $BaZr_{0.8}Pr_{0.2}O_{3-\delta}$ in dry and wet ($p_{H_2O} = 0.05$ atm) atmospheres of H_2. The bulk conductivity of $BaZr_{0.8}Y_{0.2}O_{3-\delta}$ (BZY20) and undoped $BaZrO_3$ in wet H_2 was given as reference.
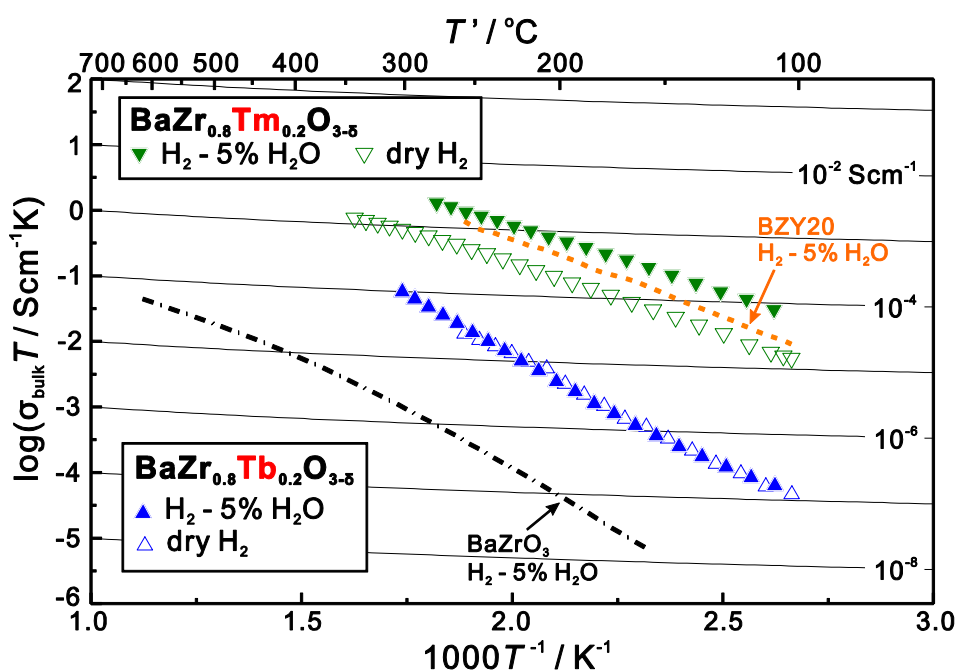
Fig. S14 Arrhenius plots of bulk conductivity of $BaZr_{0.8}Tm_{0.2}O_{3-\delta}$ and $BaZr_{0.8}Tb_{0.2}O_{3-\delta}$ in dry and wet ($p_{H_2O} = 0.05$ atm) atmospheres of H_2. The bulk conductivity of $BaZr_{0.8}Y_{0.2}O_{3-\delta}$ (BZY20) and undoped $BaZrO_3$ in wet H_2 was given as reference.

Fig. S15 Arrhenius plots of bulk conductivity of $BaZr_{0.8}Sc_{0.2}O_{3-\delta}$ and $BaZr_{0.8}Yb_{0.2}O_{3-\delta}$ in dry and wet ($p_{H_2O} = 0.05$ atm) atmospheres of H_2. The bulk conductivity of $BaZr_{0.8}Y_{0.2}O_{3-\delta}$ (BZY20) and undoped $BaZrO_3$ in wet H_2 was given as reference.
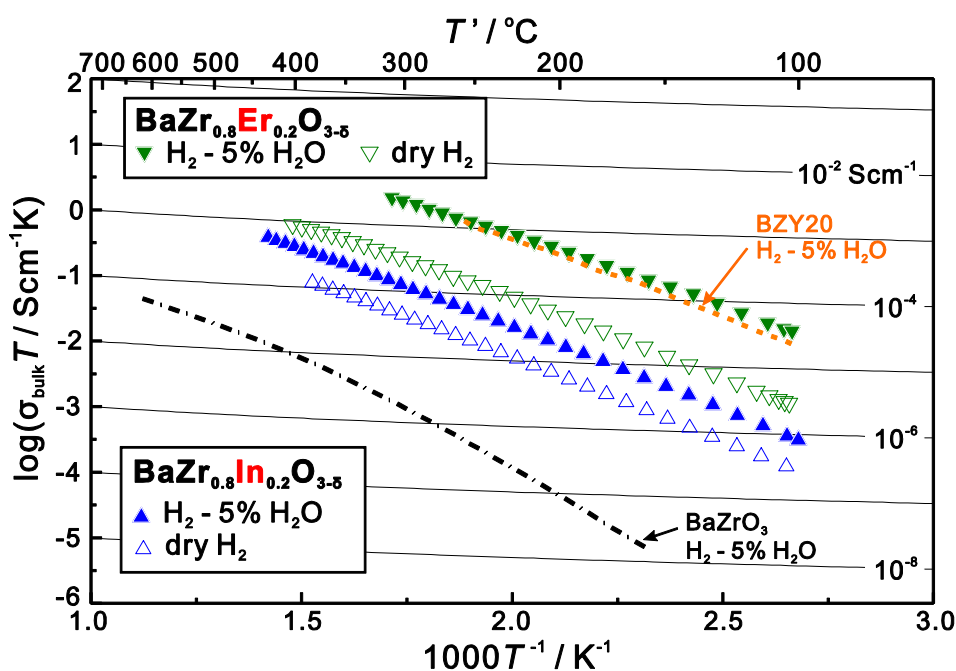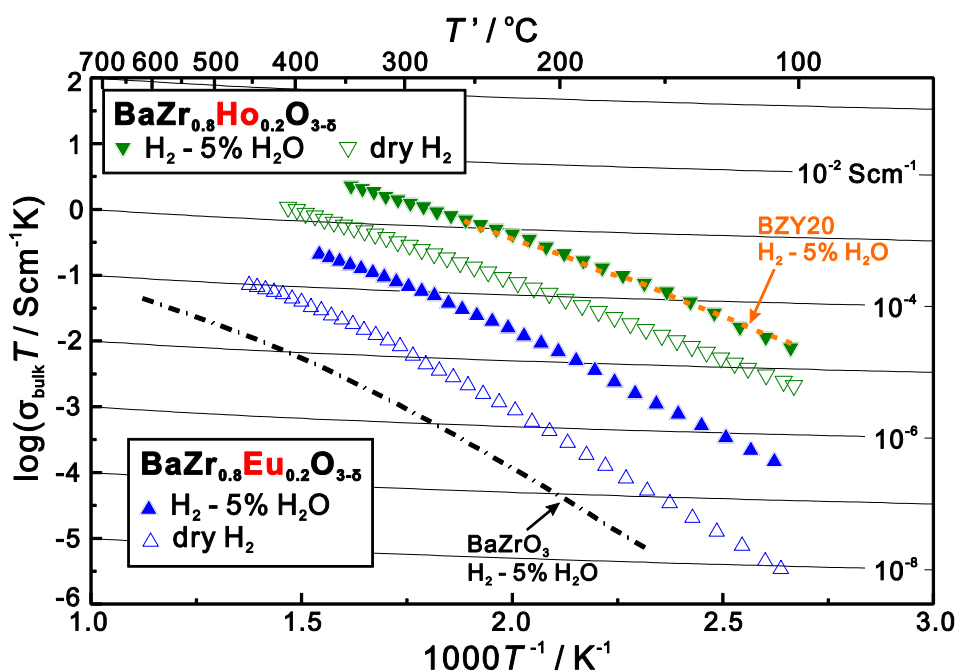

Fig. S16 Arrhenius plots of bulk conductivity of $BaZr_{0.8}In_{0.2}O_{3-\delta}$ and $BaZr_{0.8}Er_{0.2}O_{3-\delta}$ in dry and wet ($p_{H_2O} = 0.05$ atm) atmospheres of H_2. The bulk conductivity of $BaZr_{0.8}Y_{0.2}O_{3-\delta}$ (BZY20) and undoped $BaZrO_3$ in wet H_2 was given as reference.
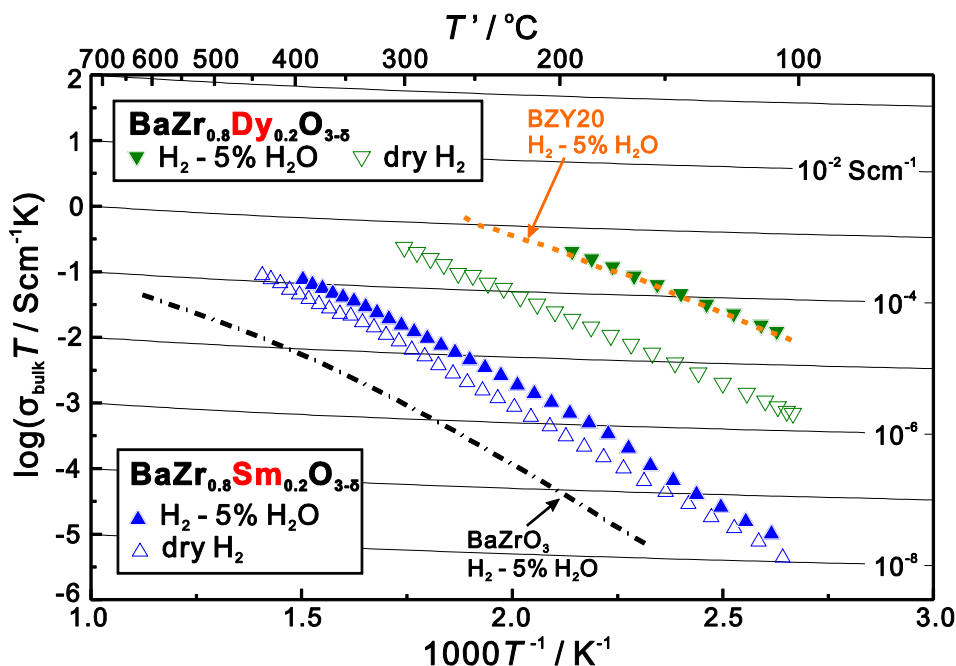
Fig. S17 Arrhenius plots of bulk conductivity of BaZr$_{0.8}$Ho$_{0.2}$O$_{3-\delta}$ and BaZr$_{0.8}$Eu$_{0.2}$O$_{3-\delta}$ in dry and wet ($p_{H_2O} = 0.05$ atm) atmospheres of H$_2$. The bulk conductivity of BaZr$_{0.8}$Y$_{0.2}$O$_{3-\delta}$ (BZY20) and undoped BaZrO$_3$ in wet H$_2$ was given as reference.

Fig. S18 Arrhenius plots of bulk conductivity of BaZr$_{0.8}$Dy$_{0.2}$O$_{3-\delta}$ and BaZr$_{0.8}$Sm$_{0.2}$O$_{3-\delta}$ in dry and wet ($p_{H_2O} = 0.05$ atm) atmospheres of H$_2$. The bulk conductivity of BaZr$_{0.8}$Y$_{0.2}$O$_{3-\delta}$ (BZY20) and undoped BaZrO$_3$ in wet H$_2$ was given as reference. The conductivities of BaZr$_{0.8}$Dy$_{0.2}$O$_{3-\delta}$ are cited from our previous works (*Solid State Ionics*, 2012, **213**, 2; *Adv. Mater.*, 2012, **24**, 2051.).

Table S1 Activation energy (E_a) and pre-exponential term (A) of the bulk conduction in the

samples of undoped $BaZrO_3$ and those doped with rare earth elements and In in dry and wet atmospheres of H_2.   The partial pressure of water vapor in the wet atmosphere was 0.05 atm.

Nominal composition	Dry H_2		$H_2 - 5\%\ H_2O$	
	E_a / eV	A / Scm^{-1}K	E_a / eV	A / Scm^{-1}K
$BaZrO_3$	0.781(3)	$4.21(33) \times 10^3$	0.760(3)	$3.30(26) \times 10^3$
$BaZr_{0.8}Sc_{0.2}O_{3-\delta}$	0.541(1)	$2.03(6) \times 10^3$	0.506(1)	$3.49(7) \times 10^3$
$BaZr_{0.8}Y_{0.2}O_{3-\delta}$	0.446(5)	$2.35(29) \times 10^3$	0.453(6)	$1.52(22) \times 10^4$
$BaZr_{0.8}In_{0.2}O_{3-\delta}$	0.510(2)	$6.19(2) \times 10^2$	0.497(3)	$1.36(11) \times 10^3$
$BaZr_{0.8}Pr_{0.2}O_{3-\delta}$	0.696(6)	$1.74(24) \times 10^3$	0.598(7)	$1.07(18) \times 10^3$
$BaZr_{0.8}Sm_{0.2}O_{3-\delta}$	0.708(2)	$1.22(7) \times 10^4$	0.738(9)	$5.53(12) \times 10^4$
$BaZr_{0.8}Eu_{0.2}O_{3-\delta}$	0.744(4)	$2.71(26) \times 10^4$	0.623(5)	$2.61(35) \times 10^4$
$BaZr_{0.8}Gd_{0.2}O_{3-\delta}$	0.599(2)	$7.92(41) \times 10^3$	0.512(3)	$9.07(74) \times 10^3$
$BaZr_{0.8}Tb_{0.2}O_{3-\delta}$	0.656(9)	$2.50(59) \times 10^4$	0.679(10)	$4.52(113) \times 10^4$
$BaZr_{0.8}Dy_{0.2}O_{3-\delta}$	0.544(2)	$1.41(6) \times 10^4$	0.497(2)	$4.76(29) \times 10^4$
$BaZr_{0.8}Ho_{0.2}O_{3-\delta}$	0.466(2)	$4.09(20) \times 10^3$	0.480(6)	$2.88(44) \times 10^4$
$BaZr_{0.8}Er_{0.2}O_{3-\delta}$	0.484(2)	$3.52(18) \times 10^3$	0.429(4)	$8.74(81) \times 10^3$
$BaZr_{0.8}Tm_{0.2}O_{3-\delta}$	0.431(3)	$3.51(24) \times 10^3$	0.400(3)	$6.32(45) \times 10^3$
$BaZr_{0.8}Yb_{0.2}O_{3-\delta}$	0.444(2)	$2.13(11) \times 10^3$	0.422(2)	$6.45(40) \times 10^3$